ChemComm

COMMUNICATION

View Article Online
View Journal | View Issue

Cite this: *Chem. Commun.*, 2024, **60**, 13546

Received 20th September 2024,
Accepted 21st October 2024

DOI: 10.1039/d4cc04873c

rsc.li/chemcomm

Wireless single-electrode electrochemiluminescence device based on wireless reverse charging or on-the-go USB transmission for multiplex analysis†

Chengda Meng,[ab] Dmytro Viktorovych Snizhko,[ac] Yuriy Tymofiiovych Zholudov,[ac] Wei Zhang,[ab] Yiran Guan,[ab] Yu Tian*[ab] and Guobao Xu*[ab]

A wireless electrochemiluminescence (ECL) device employing the wireless reverse charging function or on-the-go (OTG) USB transmission function of smartphones is designed. It was coupled with a multi-channel single-electrode electrochemical system based on the resistance-induced potential difference for multiple ECL analyses using a smartphone as the detector.

Electrochemiluminescence (ECL) needs an external power supply to induce electrochemical reaction to generate ECL. Electrochemical workstations are commonly used to supply power and record electrical response signals. However, they are expensive.[1–12] Therefore, there is an urgent need to develop portable and cost-effective ECL devices.

Wireless power transmission (WPT) is a common wireless charging technology. Compared with near field communication (NFC) technology, WPT has simpler circuits and higher power, and can achieve higher voltage and current. It was used to develop a wireless ECL device about 10 years ago.[13] In this wireless ECL device, electrodes were connected to the secondary coil of wireless transmission devices. The high-frequency alternating current (AC) makes the polarization of the electrode change between anode and cathode rapidly, resulting in weak ECL. Later a diode was connected to the secondary coil of wireless transmission devices to rectify alternating current to direct current, which prevents alternating an electrode function and enhances ECL much. However, the output voltage still fluctuates.[13–15]

Many smartphones are equipped with wireless reverse charging function, and can output stable voltage. For smartphones that do not have wireless reverse charging function, the USB transmission technology known as on-the-go (OTG) can be utilized as a power supply for an external wireless power transmitter.[16–24] So smartphones hold promise as wireless power supplies for ECL devices.

For ECL multiplex analysis, traditional electrode arrays and bipolar electrode systems have been frequently used. Both of them require the fabrication of electrode arrays to achieve multiplex analysis. The fabrication of electrode arrays is complex, costly, and not environmentally-friendly. It is also difficult to make electrode arrays for some materials. Recently, an alternative approach for ECL multiplex analysis using a single-electrode electrochemical system (SEES) based on resistance-induced potential difference has been developed. SEES consists of only one film electrode and a perforated plastic sticker, eliminating the need for the fabrication of electrode arrays.[22,25–35] Therefore, we design a new WPT device employing the wireless reverse charging function or on-the-go (OTG) USB transmission function of smartphones. The WPT device was coupled with SEES to achieve multiple detection with the advantages of simple fabrication, low cost, portability, easy operation, and so on.

The device consists of a wireless energy transmission module and the SEES. As shown in Fig. 1, the wireless transmission drive circuit consists of a receiving coil with receiver electronics (Fig. 1A) and a transmitting coil with transmitter electronics assembled on a small printed circuit board (PCB) (Fig. 1B). The driving circuit generates high frequency AC voltage at the transmitting end, and a very stable output voltage can be obtained after rectifying the induced AC voltage by rectifier circuit at the receiving end to realize a voltage supply to the single electrode system. Based on the wireless reverse charging function that many smartphones already have, the output of the wireless transmission module can directly use the wireless reverse charging function of the smartphone to supply power,

[a] *State Key Laboratory of Electroanalytical Chemistry, Changchun Institute of Applied Chemistry, Chinese Academy of Sciences, 5625 Renmin Street, Changchun 130022, China. E-mail: guobaoxu@ciac.ac.cn, tianyu@ciac.ac.cn*
[b] *School of Applied Chemistry and Engineering, University of Science and Technology of China, Hefei 230026, China*
[c] *Laboratory of Analytical Optochemotronics, Kharkiv National University of Radio Electronics, Kharkiv 61166, Ukraine*

† Electronic supplementary information (ESI) available. See DOI: https://doi.org/10.1039/d4cc04873c

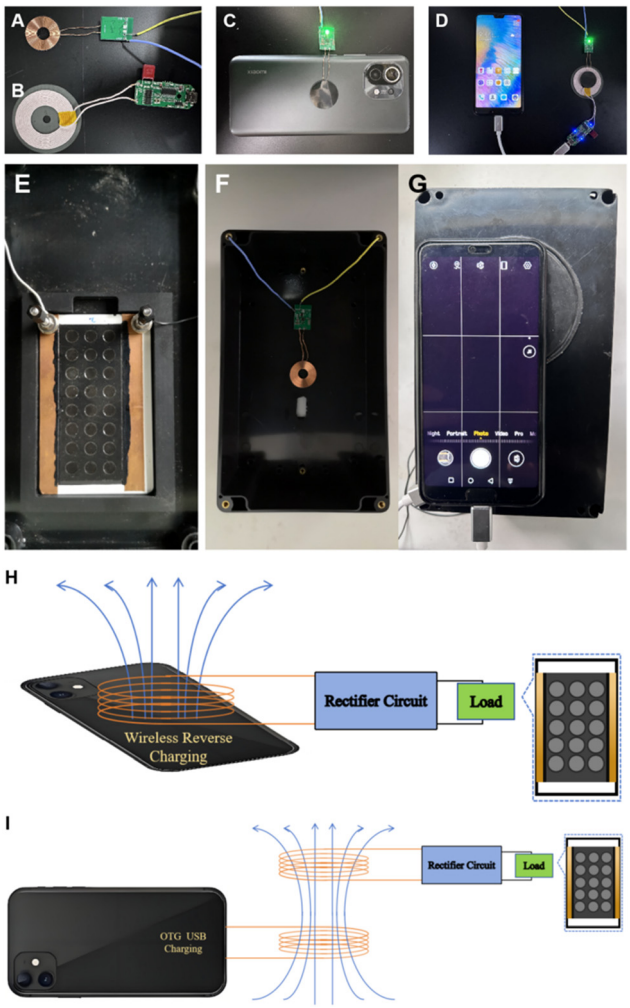

Fig. 1 Photos of the device. (A) The receiving coil with its receiver PCB; (B) the transmitting coil; (C) wireless transmission based on wireless reverse charging; (D) wireless transmission based on OTG; (E) the four-corner groove to place the SEES; (F) the receiving coil pasted on the top of the box; (G) the smartphone detects ECL emission through the opening of the box; (H) the schematic diagram of the power supply mode based on wireless reverse charging; (I) the schematic diagram of the mode based on OTG. The green LED indicates that the electrical energy is successfully transmitted to the receiver.

which greatly improves the versatility and convenience of the device (Fig. 1C). For smartphones without wireless reverse charging, the OTG (on-the-go) USB transmission function is a widely popular reverse charging technology that allows to charge other devices with smartphone *via* an OTG cable. Based on this function, power is supplied to the receiver by means of the external transmitting coil through USB connection (Fig. 1D).

The smartphone captures the device signal in a self-made small light-tight box. A four-corner groove is pasted in the middle of the box to place the SEES (Fig. 1E). The receiving coil of the wireless transmission module is directly pasted to the top of the box (Fig. 1F). At the top of the box is an opening of the same size as the protruding lens of the detection smartphone, and the position of the opening is opposite to the internal four-corner groove. To prevent light leakage at the connection between the smartphone and the opening, a dense deep black sticky gasket is pasted around the opening (Fig. 1G). The stable power supply to the internal system can be realized by placing the transmitter coil nearby to the top of the box. The box has a dimension of 200 × 115 × 75 mm. The light spot is analyzed by using a self-developed mobile application (Fig. 2). This device can detect solutions containing different concentrations of hydrogen peroxide (H_2O_2) (each row of ECL images corresponds to H_2O_2 concentration of 100, 70, 50, 20, 10, 5, 1, 0.5 μM from top to bottom) at the same time.

A schematic diagram is used to more intuitively show the power transmission in the system. As shown in Fig. 1H, for a smartphone with wireless reverse charging, the coil of the receiver can be placed directly close to the reverse side of the smartphone. The smartphone can transfer energy to the receiver through the WPT function (same connection as the actual device shown in Fig. 1C). As shown in Fig. 1I, for smartphones that do not have wireless reverse charging function, the external transmitter can be used *via* a USB OTG port (same connection as the actual device shown in Fig. 1D). The AC is transmitted wirelessly between the transmitter and the receiver. The receiver PCB transforms the high frequency AC to a stable DC potential of 5 V that is applied at the single-electrode system. A conventional rectifier with diodes can only output a unidirectional pulse voltage with a maximum value of 5 V. The potential variation by time after rectification was measured using the oscilloscope parallel to the single electrode (Fig. S1, ESI†). And this potential is considered as the external voltage

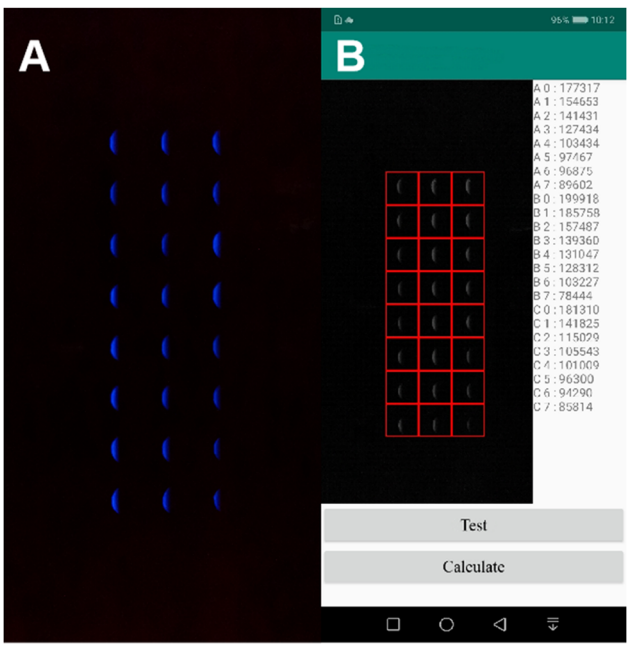

Fig. 2 ECL image analysis by the self-developed mobile application. (A) Each row of ECL images corresponds to concentrations of H_2O_2 of 100, 70, 50, 20, 10, 5, 1, and 0.5 μM from top to bottom. (B) Real-time detection based on the mobile apps. Experimental conditions: different concentrations of H_2O_2 (0.5–100 μM); 200 μM luminol in CBS buffer (pH 10).

(E_{TOT}) in the system. Powering SEES by DC is efficient for ECL signal generation for analytical purposes.

The carbon ink SEES was made using the method reported by our research group.[25,36–38] The main steps are as follows (Fig. S2A, ESI†): (1) the plastic substrate of the electrode is 54 × 86 × 0.8 mm white PVC board. The CH-8 (MOD2) carbon paste electrode was made on PVC board by a screen printing method. The size of the electrode was 40 × 77 mm and dried in a biological incubator at 37 °C. (2) The perforated polyethylene glycol terephthalate cell pattern (30 × 75 mm) is cut by the engraving machine and pasted on the carbon ink electrode. The thickness of the sticker with cell holes is 0.2 mm. The round holes of diameter 6 mm are placed on the sticker as 3 columns and 8 rows and are separated by 3 mm each of other. (3) The single-sided conductive copper tape is pasted on uncovered areas on both ends of the single electrode. (4) The connection is then coated with carbon ink to ensure the effective connection between the base screen-printing electrode and the external power supply. The connection between the single-electrode system and the wireless receiver is that the contacts drawn from opposite sides touch the surface of the copper tape to realize the power supply to the single-electrode system.

The circuit and principle of SEES are shown in Fig. S2B and C (ESI†). When an external voltage E_{tot} is applied, the current (I_{tot}) between the two copper tapes passes through the carbon ink film (I_e) and the solution in the cell (I_s). Because the resistance (R_s) of the solution is much larger than that of the carbon ink film electrode (R_e), we can consider that the current of the single electrode system is mainly through carbon ink film, and a uniform electric field is formed in SEES. H_2O_2 and dissolved oxygen on the cathode side are reduced, and luminol and H_2O_2 on the anode side are oxidized to produce ECL.

As shown in Fig. S3 (ESI†), the ECL intensity increases significantly with the increase of luminol concentration from 1 μM to 500 μM. However, when the luminol concentration reaches 200 μM, the increase of ECL intensity slows down. Therefore, the concentration of luminol was 200 μM in the subsequent experiments. Fig. S4A (ESI†) shows that the intensity of the ECL increases rapidly as the pH of the CBS buffer increases from 6 to 12. The ECL intensity increases with the increase of pH, and when the pH is 10, the ECL intensity reaches a plateau. To explore the effect of applied voltages on the ECL intensity, we customized the receiver chip PCB that is able to output different voltages (1, 2, 3, 5, 7, 10 V) and applied them to the SEES (Fig. S4B, ESI†). The ECL intensity increases rapidly with the increase of applied voltage. When the applied voltage value reaches 5 V, the ECL intensity increases slowly. Finally, the optimum luminol concentration is 200 μM, the pH is 10, and the applied voltage is 5 V.

The luminol–H_2O_2 ECL system is a common ECL pair to develop an ECL analytical system. H_2O_2 can increase the ECL intensity of luminol in the system. On this basis, we studied the device performance for H_2O_2 imaging detection. Under the optimal experimental conditions, the ECL intensities of the luminol–H_2O_2 system increase with the increase of the H_2O_2 concentration. There is a linear relationship between ECL intensity and H_2O_2 concentration in the range of 1–100 μM (Fig. 3).

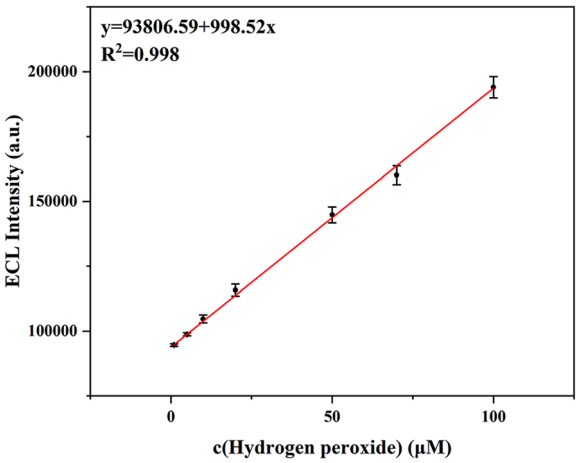

Fig. 3 Relationship curve of ECL intensity *vs.* concentration of H_2O_2. Experimental conditions: different concentrations of H_2O_2 (1–100 μM); 200 μM luminol in CBS buffer (pH 10).

The linear regression equation of signal I (ECL intensity) is I (a.u.) = 93806.59 + 998.5c (H_2O_2) [μM], and the correlation coefficient is 0.998 (n = 5). The limit of detection (LOD, S/N = 3) was found to be 0.73 μM. Compared with the existing H_2O_2 detection methods, this method has the advantages of simple operation, rapid detection, and relatively low detection limit. In comparison with previous reports for detecting H_2O_2, this method possesses comparable sensitivity (Table S1, ESI†).

To test the selectivity of this method for the detection of H_2O_2, different interfering ions and organic substances (100 μM) were added to the 100 μM H_2O_2 solutions, and the ECL intensity was recorded and compared with the blank. The obtained ECL intensity with interference is generally the same as that without interfering ions and organic substances (Fig. S5, ESI†). The error caused by each kind of interference is basically less than 5%. Therefore, the selectivity of this method for detecting H_2O_2 was successfully verified.

On the other hand, uric acid (UA) is an important analyte that can be monitored indirectly by ECL detection of H_2O_2 produced by uricase-catalyzed reactions (Fig. S6, ESI†):[39–41]

$$C_5H_4N_4O_3 + O_2 + 2H_2O \xrightarrow{\text{Uricase}} C_4H_6N_4O_3 + H_2O_2 + CO_2 \quad (1)$$

Different concentrations of UA were mixed with 200 μg mL^{-1} uricase. The mixture is mixed and reacts at room temperature (25 °C) for 10 minutes to produce hydrogen peroxide. The reacted mixture is then transported to different microelectrochemical cells of SEES for UA detection.

The catalytic reaction conditions of UA were optimized by first studying the effect of pH on the reaction system. According to the characteristics of uricase, as shown in Fig. S7A (ESI†), the ECL intensity is low when pH ≤ 7. In the pH range of 7–11, the catalytic activity of uricase is high and has good stability in solution. The ECL emission produced after the catalytic reaction reaches a maximum and enters a plateau after the pH reaches 10. In the subsequent experiments, the CBS used in the reaction system had a pH of 10.

In the second step, we investigated the effect of the UA catalytic reaction time on ECL intensity. As shown in Fig. S7B (ESI†), the intensity of ECL increases during the reaction. When the reaction time reaches 10 minutes, ECL intensity saturation has been observed. To obtain better sensitivity and to minimize analysis duration, the catalytic reaction system was observed over 10 minutes in subsequent experiments.

As shown in Fig. S8 (ESI†), the linear range of UA detected is 5–100 μM, and the LOD is 1.32 μM. The linear regression equation of signal I is I (a.u.) = 84045.94 + 992.55c (UA) [μM], and the correlation coefficient is 0.997 (n = 5). In order to investigate the selectivity of the method, control experiments were carried out with biomolecules like different kinds of amino acids and other potential interferents (Fig. S9, ESI†). 100 μM of UA produced a higher ECL response, while the signals of other compounds were relatively small and negligible. In comparison with previous reports for detecting UA, this method possesses comparable sensitivity (Table S2, ESI†).

In summary, we designed a new type of ECL detection device employing the wireless reverse charging function or on-the-go (OTG) USB transmission function of most smartphones. At the same time, we introduce SEES to realize the simultaneous detection of multi-concentration and a multi-analyte detection system. In addition, to improve the convenience and reduce the cost of the device, we integrate the above system into a small box to achieve real-time detection. The wireless reverse transmission function of the smartphone provides a more convenient way to transmit energy for ECL. The ECL images obtained by the device were analyzed in real time in the self-made mobile phone application to determine H_2O_2 and UA sensitively. The device has the advantages of low cost, low power consumption, and ease of use. It holds great promise for ECL detection, including multiplex analysis and point-of-care testing.

This project was kindly supported by the Ministry of Science and Technology of the People's Republic of China (No. 2023YFE0201800, CU03-02), National Natural Science Foundation of China (No. 22174136, 22004116, and 22204160), and Natural Science Foundation of Jilin Province (No. YDZJ202201ZYTS341).

Data availability

The data supporting this article have been included as part of the ESI.†

Conflicts of interest

There are no conflicts to declare.

References

1 Z. Liu, W. Qi and G. Xu, *Chem. Soc. Rev.*, 2015, **44**, 3117–3142.
2 K. Nagano, Y. Terada, A. Araki, S. Osaki, M. Saito and E. Tamiya, *Electroanal*, 2022, **34**, 8–14.
3 Y. Lu, Y. Ning, B. Li and B. Liu, *Anal. Chem.*, 2023, **96**, 463–470.
4 P. Zhou, W. Fu, L. Ding, Y. Yan, W. Guo and B. Su, *Electrochim. Acta*, 2023, **439**, 141716.
5 Y. Wang, G. Zhao, H. Chi, S. Yang, Q. Niu, D. Wu, W. Cao, T. Li, H. Ma and Q. Wei, *J. Am. Chem. Soc.*, 2021, **143**, 504–512.
6 M. Feng, A. L. Dauphin, L. Bouffier, F. Zhang, Z. Wang and N. Sojic, *Anal. Chem.*, 2021, **93**, 16425–16431.
7 M. Tan, Y. Wang, Z. Hong, P. Zhou, J. Jiang and B. Su, *Analyst*, 2024, **149**, 1496–1501.
8 A. Barhoum, Z. Altintas, K. S. S. Devi and R. J. Förster, *Nano Today*, 2023, **50**, 101874.
9 C. Meng, S. Knezevic, F. Du, Y. Guan, F. Kanoufi, N. Sojic and G. Xu, *eScience*, 2022, **2**, 591–605.
10 W. Gu, X. Wang, M. Xi, X. Wei, L. Jiao, Y. Qin, J. Huang, X. Cui, L. Zheng, L. Hu and C. Zhu, *Anal. Chem.*, 2022, **94**, 9459–9465.
11 N. S. Adamson, A. G. Theakstone, L. C. Soulsby, E. H. Doeven, E. Kerr, C. F. Hogan, P. S. Francis and L. Dennany, *Chem. Sci.*, 2021, **12**, 9770–9777.
12 K. Hiramoto, K. Ino, K. Komatsu, Y. Nashimoto and H. Shiku, *Biosens. Bioelectron.*, 2021, **181**, 113123.
13 W. Qi, J. Lai, W. Gao, S. Li, S. Hanif and G. Xu, *Anal. Chem.*, 2014, **86**, 8927–8931.
14 E. Villani, N. Shida and S. Inagi, *Electrochim. Acta*, 2021, **389**, 138718.
15 M. Liu, G. Salinas, J. Yu, A. Cornet, H. Li, A. Kuhn and N. Sojic, *Chem. Sci.*, 2023, **14**, 10664–10670.
16 S. M. Khoshfetrat, H. Khoshsafar, A. Afkhami, M. A. Mehrgardi and H. Bagheri, *Anal. Chem.*, 2019, **91**, 6383–6390.
17 A. Shafaat, R. Zalneravicius, D. Ratautas, M. Dagys, R. Meskys, R. Rutkiene, J. F. Gonzalez-Martinez, J. Neilands, S. Bjorklund, J. Sotres and T. Ruzgas, *ACS Sens.*, 2022, **7**, 1222–1234.
18 D. Snizhko, Y. Zholudov, A. Kukoba and G. Xu, *J. Electroanal. Chem.*, 2023, **936**, 117380.
19 Y. Wang, R. Jin, N. Sojic, D. Jiang and H. Chen, *Angew. Chem., Int. Ed.*, 2020, **59**, 10416–10420.
20 A. L. Dauphin, S. Arbault, A. Kuhn, N. Sojic and L. Bouffier, *Chem. Phys. Chem.*, 2020, **21**, 600–604.
21 G. Salinas, G. Bonetti, R. Cirilli, T. Benincori, A. Kuhn and S. Arnaboldi, *Electrochim. Acta*, 2022, **421**, 140494.
22 S. F. Douman, E. Brennan, E. I. Iwuoha and R. J. Förster, *Anal. Chem.*, 2017, **89**, 11614–11619.
23 L. Koefoed, S. U. Pedersen and K. Daasbjerg, *Curr. Opin. Electrochem.*, 2017, **2**, 13–17.
24 L. Qi, Y. Xia, W. Qi, W. Gao, F. Wu and G. Xu, *Anal. Chem.*, 2016, **88**, 1123–1127.
25 F. Du, Z. Dong, F. Liu, S. Anjum, M. Hosseini and G. Xu, *Electrochim. Acta*, 2022, **420**, 140431.
26 A. Firoozbakhtian, M. Hosseini, Y. Guan and G. Xu, *Anal. Chem.*, 2023, **95**, 15110–15117.
27 M. Bhaiyya, P. K. Pattnaik and S. Goel, *Microfluid. Nanofluid.*, 2021, **25**, 02442.
28 E. Vidal, C. E. Domini, D. C. Whitehead and C. D. Garcia, *Sens Diagn.*, 2022, **1**, 496–503.
29 Y. Shi, E. Villani, Y. Chen, Y. Zhou, Z. Chen, A. Hussain, G. Xu and S. Inagi, *Anal. Chem.*, 2023, **94**, 1532–1540.
30 M. L. Bhaiyya, S. Gangrade, P. K. Pattnaik and S. Goel, *IEEE Trans. Instrum. Meas.*, 2022, **71**, 3036642.
31 G. Ma, J. Zhou, C. Tian, D. Jiang, D. Fang and H. Chen, *Anal. Chem.*, 2013, **85**, 3912–3917.
32 M. Bhaiyya, P. Rewatkar, P. K. Pattnaik and S. Goel, *J. Micromech. Microeng.*, 2023, **33**, 024001.
33 W. Guo, H. Ding, C. Gu, Y. Liu, X. Jiang, B. Su and Y. Shao, *J. Am. Chem. Soc.*, 2018, **140**, 15904–15915.
34 G. Valenti, S. Scarabino, B. Goudeau, A. Lesch, M. Jovic, E. Villani, M. Sentic, S. Rapino, S. Arbault, F. Paolucci and N. Sojic, *J. Am. Chem. Soc.*, 2017, **139**, 16830–16837.
35 Y. Kim, H. Kim, J. B. Son, M. Filatov, C. H. Choi, N. K. Lee and D. Lee, *Angew. Chem., Int. Ed.*, 2023, **62**, e202302107.
36 W. Gao, K. Muzyka, X. Ma, B. Lou and G. Xu, *Chem. Sci.*, 2018, **9**, 3911–3916.
37 F. Du, Z. Dong, Y. Guan, A. M. Zeid, D. Ma, J. Feng, D. Yang and G. Xu, *Anal. Chem.*, 2022, **94**, 2189–2194.
38 X. Ma, L. Qi, W. Gao, F. Yuan, Y. Xia, B. Lou and G. Xu, *Electrochim. Acta*, 2019, **308**, 20–24.
39 H. Mizuguchi, S. Fujiki, T. Shibata, M. Oishi, M. Liyama, T. Takayanagi, Y. Lin and M. Yeh, *Sens. Actuators, B*, 2023, **383**, 133588.
40 Y. Zhang, L. Guo, Y. Yu and J. Wang, *Anal. Chem.*, 2020, **92**, 15699–15704.
41 D. Zhao, G. Yu, K. Tian and C. Xu, *Biosens. Bioelectron.*, 2016, **82**, 119–126.